J Mol Model (2013) 19:3705–3717
DOI 10.1007/s00894-013-1903-z

ORIGINAL PAPER

Computational study of decomposition mechanisms and thermodynamic properties of molecular-type cracking patterns for the highly energetic molecule GZT

Sou-Ro Cheng · Ken-Fa Cheng · Min-Hsien Liu · Yaw-Shun Hong · Cheng Chen

Received: 13 April 2013 / Accepted: 28 May 2013 / Published online: 19 June 2013
© Springer-Verlag Berlin Heidelberg 2013

Abstract This study uses the Gaussian 03 program and density functional theory B3LYP with three basis set methods—[B3LYP/6-311+G(d,p), B3LYP/6-31+G(2d,p), and B3LYP/6-31G(d,p)]—to model the highly energetic ionic compound diguanidinium 5,5′-azotetrazolate (GZT) to research its decomposition mechanisms and thermodynamic properties. Molecular-type cracking patterns are proposed, which were initiated by heterocyclic ring opening, sequential cracking of the two five-membered rings of GZT, and simultaneous release of N_2 molecules; whereas proton transfer, bond-breaking, and atomic rearrangements were performed subsequently. Finally, 15 reaction paths and five transition states were obtained. All possible decomposition species and transition states, including intermediates and products, were identified, and their corresponding enthalpy and Gibbs free energy values were obtained. The results revealed that (1) the maximum activation energy required is 187.8 kJ mol^{-1}, and the enthalpy change (ΔH) and Gibbs free-energy change (ΔG) of the net reaction are −525.1 kJ mol^{-1} and −935.6 kJ mol^{-1}, respectively; (2) GZT can release large amounts of energy, the main contribution being from the disintegration of the 5,5'-azotetrazolate anion (ZT^{2-}) skeleton (ΔH=−598.3 kJ mol^{-1}); and (3) the final products contained major amounts of N_2 gas, but remaining gas molecules such as HCN and NH_3 were obtained, which are in agreement with experimental results. The detailed decomposition simulation results demonstrated the feasibility of this method to calculate the energies of the thermodynamic reactions for the highly energetic GZT and predict the most feasible pathways and the final products.

Keywords Decomposition mechanism · GZT · Heterocyclic ring opening · High nitrogen energetic material · Molecular type cracking pattern

S.-R. Cheng
School of Defense Science, Chung Cheng Institute of Technology National Defense University, Tahsi, Taoyuan 33509, Taiwan, Republic of China

K.-F. Cheng · M.-H. Liu · Y.-S. Hong (✉) · C. Chen
Department of Chemical and Material Enginnering, Chung Cheng Institute of Technology National Defense University, Tahsi, Taoyuan 33509, Taiwan, Republic of China
e-mail: yshong@ndu.edu.tw

Introduction

5,5'-azotetrazolate anion (ZT^{2-}) combines with guanidinium, aminoguanidinium, diaminoguanidinium, and triaminoguanidinium cations to form diguanidinium 5,5'-azotetrazolate (GZT) and its derivatives (shown in Fig. 1), such as diaminoguanidinium 5,5'-azotetrazolate (AGZT), bis(diaminoguanidinium) 5,5'-azotetrazolate (DAGZT), and bis(triaminoguanidinium) 5,5'-azotetrazolate (TAGZT), respectively, which have been reported to be highly energetic and stable ionic materials [1–3]. This series of nonmetal salts containing a considerably higher mass percentage of nitrogen but a lower carbon-hydrogen content with a high positive heat of formation [4–6] are energetic nitrogen-rich compounds. These salts are potential ingredients of gun propellants and gas generators. Unlike conventional energetic material explosives such as TNT, RDX, and HMX, GZT and its derivatives can derive energy from the combination of a high heat of formation and generation of a large volume of gases (mainly nitrogen) at the appropriate energy detonated under fast decomposition reactions, with a tremendous potential for application [7–12]. Furthermore, GZT and its derivatives have the characteristics of an appropriate stability against impact, friction, and heat [3, 4]. Significant research has been performed on GZT and its derivatives, and a large number of studies have investigated its synthesis and characterization in the past decade [13–19].

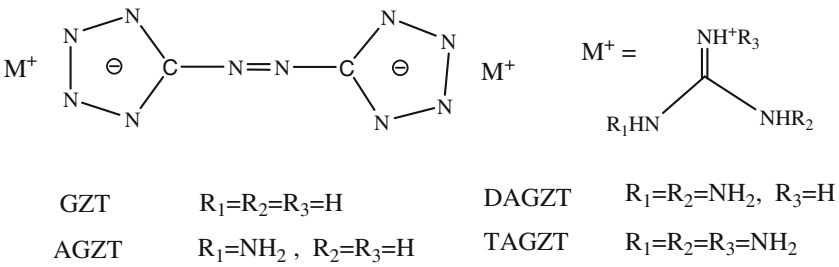

Fig. 1 Structures of GZT and its derivatives (AGZT, DAGZT, and TAGZT)

In recent years, more reports have been published about the decomposition mechanisms of GZT and its derivatives [20–25], and Dames et al. also proposed heterocyclic ring opening via proton transfer-type decomposition mechanisms of GZT to interpret the experimental results [24]. Because the instantaneous explosion pyrolysis process is complicated in high energetic compound experiments, and the fundamental reactions cannot be observed and obtained, the experimental final products measurement can only be used to infer the possible decomposition reaction paths. Alavi et al. claimed that: "Theoretical calculations can play a crucial role in resolving the details not available from experiments." [26]. However, only a few studies have been published on simulation calculations and speculation about the thermodynamic properties and decomposition mechanisms of this series of compounds.

Our laboratory proposed an ionic-type fragmentation pattern of the decomposition of GZT previously, and the theoretical simulation results revealed that the ZT^{2-} anion and the G^{+} cation individual subsequently decomposed, requiring large activation energies of 477 kJ mol^{-1} and 752 kJ mol^{-1}, respectively [27]. This result motivated us to perform a new investigation into the theoretical unimolecular decomposition mechanisms of GZT. It is believed that the stability of

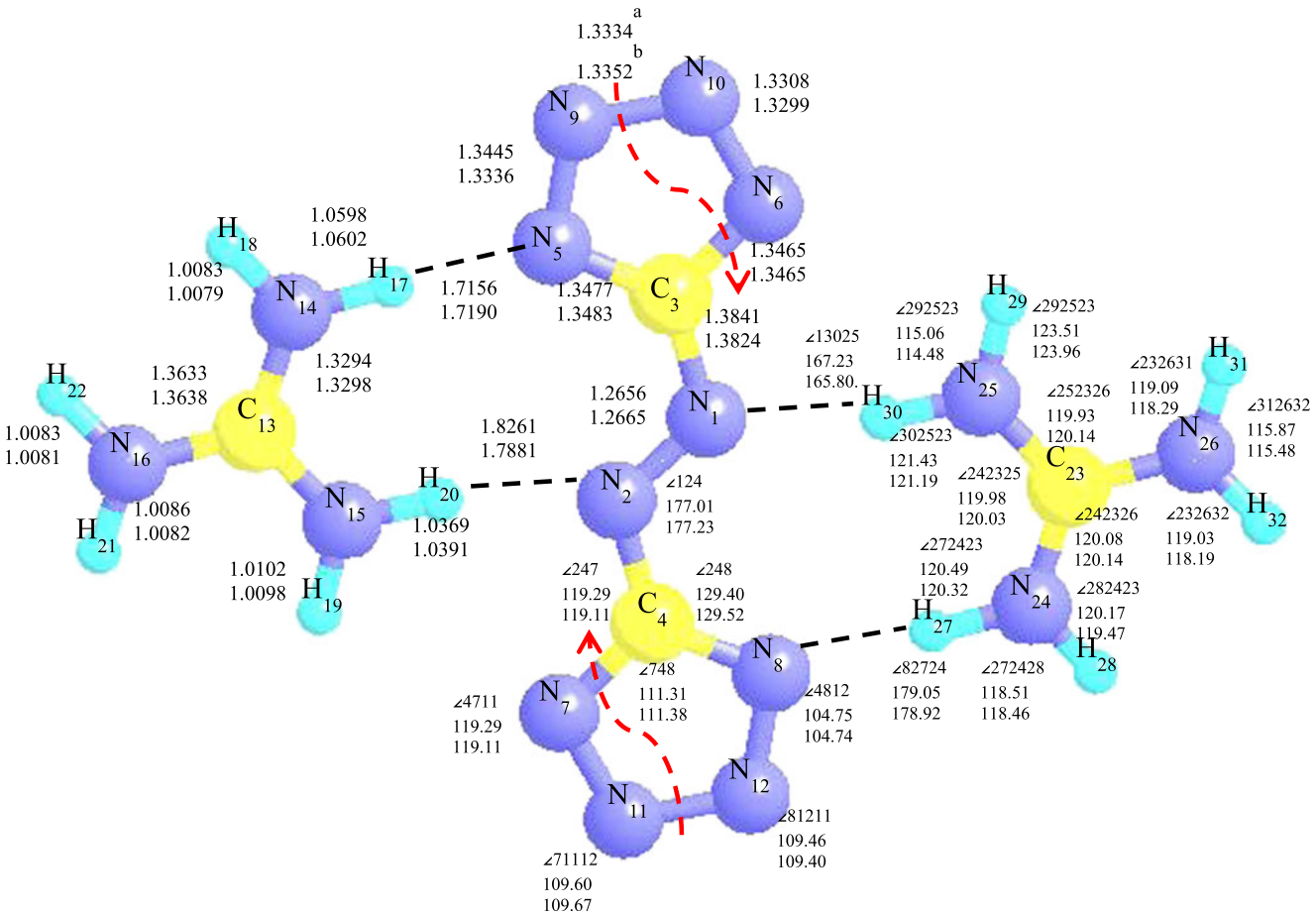

Fig. 2 The bond distance and bond angles of the GZT molecular structure with a Ci group (distance in Å). (a) results by B3LYP/6-31++G(d,p) and B3LYP/6-31+G(d,p); (b) result by B3LYP/6-31G (d,p) ref [28].

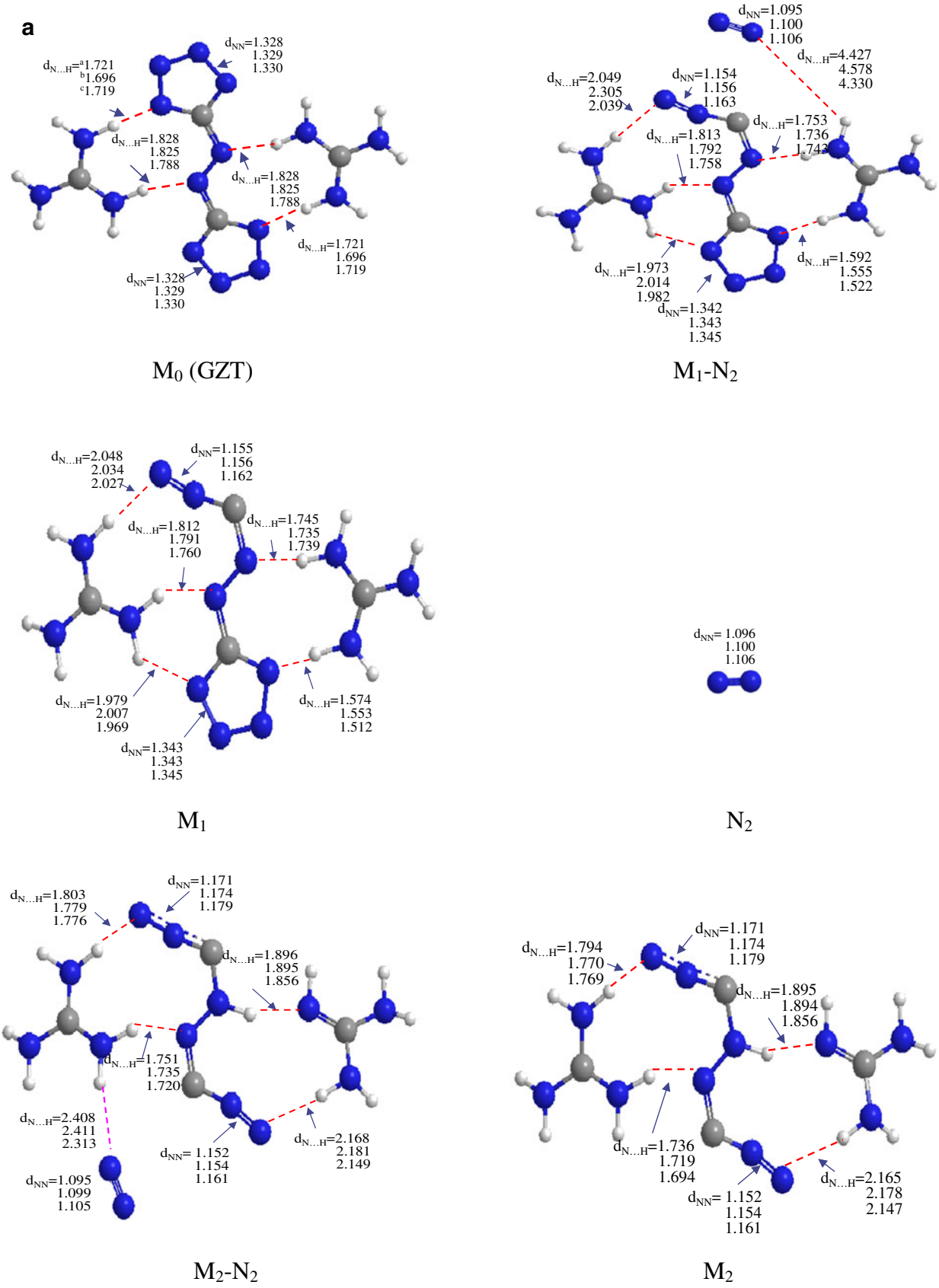

Fig. 3 Optimized geometries of decomposition species of GZT. (a) B3LYP/6-311+G(d,p) calculated results, (b) B3LYP/6-31+G(2d,p) calculated results, (c) B3LYP/6-31G(d,p) calculated results, in Å

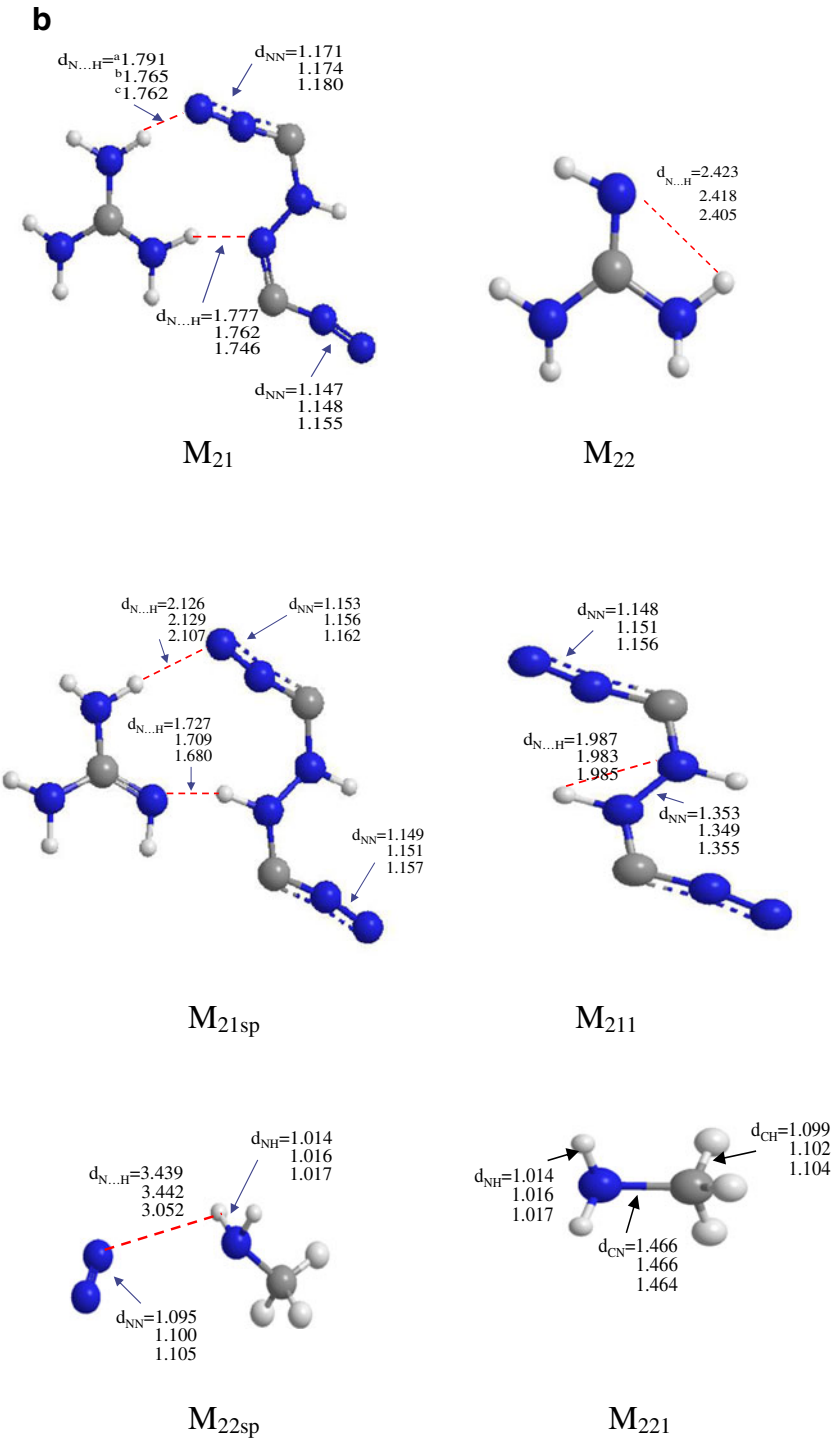

Fig. 3 (continued)

GZT is mostly attributed to the attraction forces between the guanidinium cation (G^+) and ZT^{2-} anion and corresponds partly to localized hydrogen bonding [3, 28, 29]. Storm et al. and Politzer et al. proposed the heterocyclic ring opening of triazoles, through the elimination of N_2, as the initial step of the decomposition mechanism [30, 31]. As mentioned above, based on the assumptions, by the principle of weaker bonding corresponding to easier cleavage, and more stable small molecules (for example N_2) are formed. We propose a new molecular-type cracking patterns decomposition mechanism

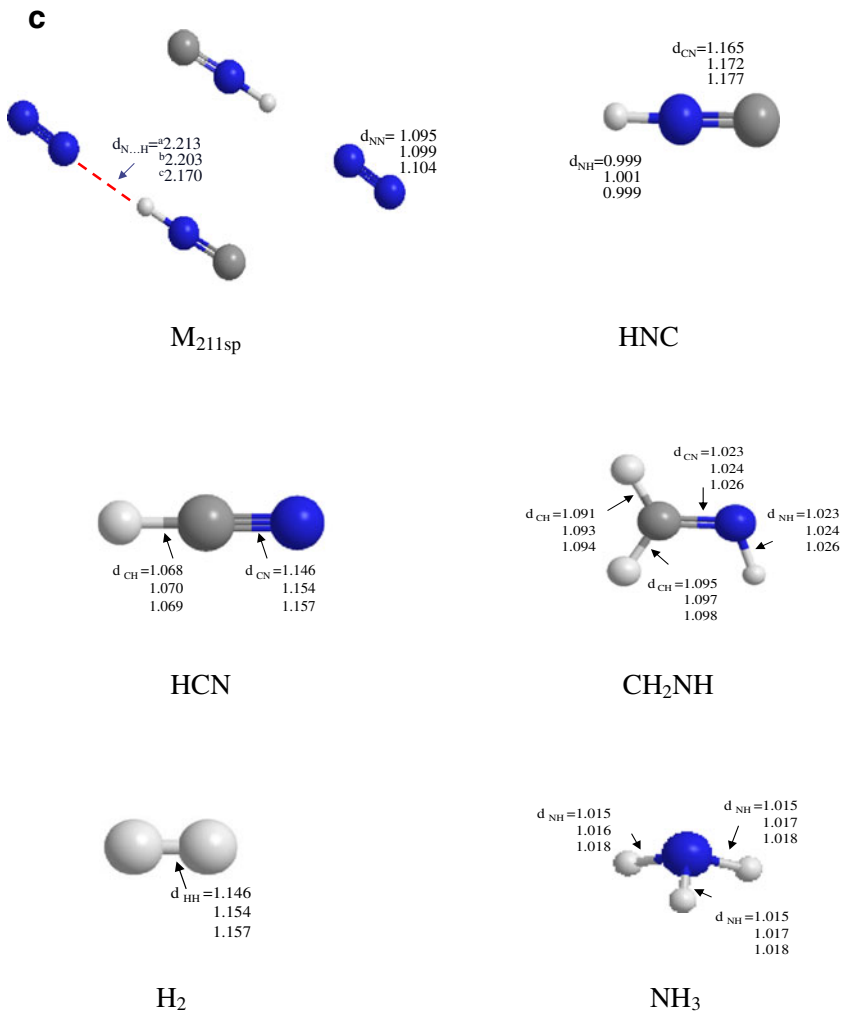

Fig. 3 (continued)

of GZT, in which Coulomb attraction forces and hydrogen bonding between the guanidinium cation (G^+) and ZT^{2-} anion were taken into account and retained. The patterns were initiated by heterocyclic ring opening, sequential cracking of the N-N bond (1.3352 Å) and C-N bond (1.3465 Å) of the two five-membered rings of GZT (shown in Fig. 2), and simultaneous release of N_2 molecules. The detailed decomposition paths and the thermodynamic properties are discussed in this research.

Computation

Geometrical optimization

The Gaussian 03 program [32] and density functional theory B3LYP [33] with three basis set methods B3LYP/6-311+G(d,p), B3LYP/6-31+G(2d,p), and B3LYP/6-31G(d,p) were adopted to calculate the optimized geometries of GZT and its decomposition species.

Modeling of transition states

The transition state species were modeled with the B3LYP/6-31+G(2d,p) and B3LYP/6-31G(d,p) approaches and were then identified by applying the QST3(or QST2)-type optimization procedure in the program [34, 35].

Calculation of thermodynamic energy

For GZT, the decomposition intermediates, transition states via the zero-point energy calculation and thermodynamic values for the internal energy U (0 K), enthalpy H (298 K), and free energy G (298 K) can be manually obtained. The activation

Table 1 Thermodynamic energy of decomposition species of GZT

species	B3LYP/6-311+G(d,p)				B3LYP/6-31+G(2d,p)				B3LYP/6-31G(d,p)			
	E_{SCF}	U (0 K)	H (298 K)	G (298 K)	E_{SCF}	U (0 K)	H (298 K)	G (298 K)	E_{SCF}	U (0 K)	H (298 K)	G (298 K)
M_0	−1035.91035	−1035.67431	−1035.6524	−1035.72675	−1035.67164	−1035.43465	−1035.41282	−1035.48660	−1035.60429	−1035.36665	−1035.34492	−1035.41873
M_1-N_2	−1035.88506	−1035.65621	−1035.63105	−1035.71665	−1035.63748	−1035.40833	−1035.38301	−1035.47037	−1035.56688	−1035.33705	−1035.31209	−1035.39725
M_1	−926.31977	−926.09732	−926.07633	−926.14834	−926.10409	−925.88081	−925.85992	−925.93134	−926.04093	−925.81744	−925.79662	−925.86838
M_2-N_2	−926 .28793	−926.06993	−926.04515	−926.13049	−926.06416	−925.84574	−925.82097	−925.90597	−925.99599	−925.77630	−925.75184	−925.83549
M_2	−816.72225	−816.51081	−816.49007	−816.56252	−816.52838	−816.31717	−816.29640	−816.36892	−816.46793	−816.25496	−816.23449	−816.30612
M_{21}	−611.25765	−611.12357	−611.10889	−611.16561	−611.11355	−610.97928	−610.96450	−611.02175	−611.06878	−610.93374	−610.919208	−610.97538
M_{21sp}	−611.25418	−611.11872	−611.10415	−611.16219	−611.10639	−610.97417	−610.95963	−611.01700	−611.06540	−610.92904	−610.91464	−610.97126
M_{22}	−205.45031	−205.37458	−205.3691	−205.40094	−205.40063	−205.32479	−205.31931	−205.35116	−205.37942	−205.30317	−205.29774	−205.32951
M_{22sp}	−205.45960	−205.38985	−205.38111	−205.42652	−205.40585	−205.33648	−205.32773	−205.37364	−205.38905	−205.31862	−205.31011	−205.35316
M_{211}	−405.78016	−405.72158	−405.71302	−405.75393	−405.68480	−405.62609	−405.61751	−405.65846	−405.65610	−405.59705	−405.58853	−405.62995
M_{211sp}	−406.00154	−405.95642	−405.94091	−406.00393	−405.89528	−405.850045	−405.83486	−405.89672	−405.86075	−405.81441	−405.79928	−405.86016
M_{221}	−95.89583	−95.83205	−95.82766	−95.85499	−95.87312	−95.80929	−95.80491	−95.83222	−95.86369	−95.79949	−95.795151	−95.82239
N_2	−109.56348	−109.55793	−109.55463	−109.57636	−109.53269	−109.52721	−109.52391	−109.54565	−109.52413	−109.51853	−109.51523	−109.53698
HNC	−93.43329	−93.41794	−93.41405	−93.437450	−93.41080	−93.39527	−93.39146	−93.41479	−93.40011	−93.38442	−93.38062	−93.40394
CH_2NH	−94.66499	−94.62522	−94.62136	−94.64713	−94.64154	−94.60253	−94.59867	−94.62445	−94.63346	−94.59347	−94.58961	−94.61539
HCN	−93.45449	−93.43813	−93.43465	−93.45749	−93.43142	−93.41551	−93.41201	−93.43488	−93.42458	−93.40812	−93.40464	−93.42749
H_2	−1.17957	−1.16950	−1.16620	−1.18099	−1.17742	−1.16837	−1.16506	−1.17985	−1.17854	−1.16837	−1.165061	−1.179853
NH_3	−56.58384	−56.54961	−56.54580	−56.56868	−56.56833	−56.53432	−56.53051	−56.55339	−56.55777	−56.52333	−56.51953	−56.54241

*$E_{SCF,}$ U (thermal energy), H (thermal enthalpy), G (Gibbs free energy) (in au)

energy can be obtained from the energy difference between the reactants and the transition states; internal energy change ΔU (0 K), enthalpy energy change ΔH (298 K), and Gibbs free-energy change ΔG (298 K) can also be obtained from the energy differences between the reactants and the products.

Results and discussion

Optimized structures

For convenient description, GZT is named M_0, while the various intermediates in the decomposition reaction are named M_1-N_2, M_1, M_2-N_2, M_2 …etc. All of the species (M_1-N_2, M_1, M_2-N_2,…etc.) formed in the thermal decomposition of GZT were modeled as stable with real positive frequencies. The optimized structures of the decomposition species and the corresponding enthalpy and Gibbs free energy were successfully obtained, as shown in Fig. 3 and Table 1. The thermodynamic energies of the reaction paths of GZT decomposition were calculated and are listed in Table 2.

Calculation of transition states

After local minima calculation for the above-mentioned 15 reactions was completed, the transition state of each reaction was calculated using synchronous transit-guided quasi-Newton (STQN)-type calculations [34, 35]. In this work the quadratic synchronous transit approach with the QST3 option, implying the geometrical data of suitable reactants, products, and assigned initial inferred transition state, was applied to the optimization procedure of the transition states. This method converges efficiently when provided with an empirical estimate of the Hessian and suitable starting structures [34]. In order to prove the transition states to be the saddle point with only one imaginary frequency, vibration frequency calculation was followed by geometrical optimization calculation. Only five transition states were successfully identified, and were defined as TS_{01}, TS_{12dc}, TS_{2dc}, TS_{21dc}, and TS_{22dc}, as shown in Fig. 4. All thermodynamic energies and activation energies for the transition states are listed in Tables 3 and 4.

Molecular-type cracking patterns

Molecular-type cracking patterns are proposed, which were initiated by heterocyclic ring opening, sequential cracking of the N-N bond (1.3352 Å) and C-N bond (1.3465 Å) of the two five-membered rings of GZT (shown in Fig. 2), and simultaneous release of N_2 molecules. Proton transfer, bond breaking, and atomic rearrangements were performed subsequently. Finally, 15 reaction paths and five transition states were obtained. The molecular-type cracking patterns are shown in Fig. 5, and are described as follows:

Path 1:The N-N bond and C-N bond of the first five-membered ring in M_0 (GZT) are broken, and M_1-N_2 are

Table 2 Thermodynamic energy of decomposition reaction paths of GZT

Path	Reaction	B3LYP/6-311+G(d,p)			B3LYP/6-31+G(2d,p)			B3LYP/6-31G(d,p)		
		*ΔU (0 K)	ΔH (298 K)	ΔG (298 K)	ΔU (0 K)	ΔH (298 K)	ΔG (298 K)	ΔU (0 K)	ΔH (298 K)	ΔG (298 K)
1	$M_0 \rightarrow M_1$-N_2	47.5	56.1	26.5	69.1	78.3	42.6	77.7	86.2	56.4
2	M_1-$N_2 \rightarrow M_1 + N_2$	2.5	0.2	−21. 2	0.8	−2.1	−17.4	2.8	0.6	−21.3
3	$M_1 \rightarrow M_2$-N_2	71.9	81.9	46.9	92.1	102.3	66.6	108	117.6	86.4
4	M_2-$N_2 \rightarrow M_2 + N_2$	3.1	1.2	−22	3.6	1.7	−22.6	7.4	5.6	−20
5	$M_2 \rightarrow M_{21} + M_{22}$	33.2	31.7	−10.6	34.4	33.1	−10.5	47.4	46.1	3.2
6	$M_{21} \rightarrow M_{21sp}$	12.7	12.4	8.9	13.4	12.8	12.5	12.4	12	10.8
7	$M_{21sp} \rightarrow M_{211} + M_{22}$	59.3	57.9	19.2	61.1	59.9	19.4	75.7	74.5	31
8	$M_{22} \rightarrow M_{22sp}$	−40.1	−31.6	−67.2	−30.7	−22.1	−59	−40.6	−32.5	−61.2
9	$M_{22sp} \rightarrow M_{221} + N_2$	2.8	0.7	−21.6	2.2	−0.2	−20	5.1	3.1	−20.7
10	$M_{211} \rightarrow M_{211sp}$	−617	−598.3	−656.4	−587.9	−570.7	−625.5	−570.7	−553.3	−604.4
11	$M_{211sp} \rightarrow 2N_2 + 2HNC$	12.3	9.3	−62.5	13.3	10.8	−63.4	22.3	19.9	−56.9
12	$HNC \rightarrow HCN$	−53	−54.1	−52.5	−53.1	−53.9	−52.8	−62.2	−63.1	−61.9
13	$M_{221} \rightarrow CH_2NH + H_2$	157.5	164.9	130.1	100.8	108.2	73.3	98.9	106.3	71.3
14	$CH_2NH \rightarrow HCN + H_2$	46	53.7	22.5	49	56.7	25.5	44.6	52.3	21.1
15	$3H_2 + N_2 \rightarrow 2NH_3$	−79.7	−94.4	−41	−95.4	−110.1	−56.6	−60.5	−75.2	−21.7

*ΔU (thermal energy), ΔH (thermal enthalpy), ΔG (Gibbs free energy) (in kJ mol^{-1})

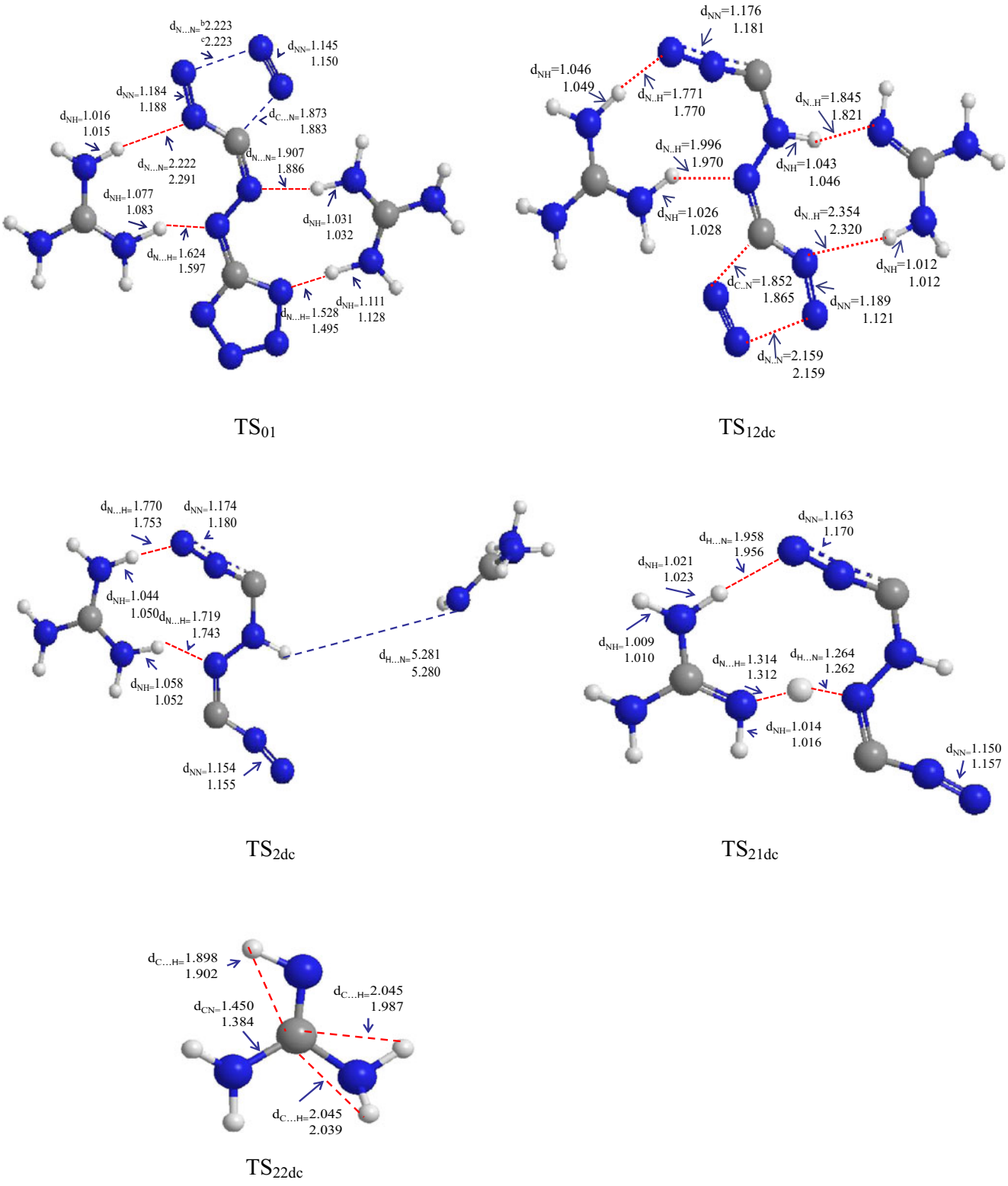

Fig. 4 Optimized geometries of transition state species of GZT. (b) B3LYP/6-31+G(2d,p) calculated results, (c) B3LYP/6-31G(d,p) calculated results, in Å

obtained; Path 2: M_1-N_2 overcomes the weak van der Waals forces (3.244 Å, 3.368 Å) to release an N_2 molecule to form M_1; Path 3: M_1, as in path 1, the second five-membered ring opening forms M_2-N_2, and proton transfer simultaneously occurs; Path 4: M_2-N_2 also overcomes the weak van der Waals forces (3.414 Å, 4.683 Å) to release an N_2 molecule

Table 3 Thermodynamic energy of transition state species of GZT

Species	B3LYP/6-31+G(2d,p)				Only one imaginary frequency ν – (cm^{-1})	B3LYP/6-31G(d,p)				Only one imaginary frequency ν (cm^{-1})
	*E_{SCF}	U (0 K)	H (298 K)	G (298 K)		E_{SCF}	U (0 K)	H (298 K)	G (298 K)	
TS_{01}	−1035.63747	−1035.37500	−1035.35208	−1035.42877	−322.45641	−1035.53823	−1035.30789	−1035.28505	−1035.36205	−315.59561
TS_{12dc}	−926.031964	−925.81194	−925.78954	−925.86554	−353.39962	−925.96853	−925.74722	−925.72511	−925.80022	−344.48772
TS_{2dc}	−816.529085	−816.31716	−816.29640	−816.36889	−10.81243	−816.44752	−816.23616	−816.21818	−816.28675	−23.61393
TS_{21dc}	−611.106203	−610.97482	−610.96072	−611.01632	−1064.47875	−611.06235	−610.93020	−610.91624	−610.97135	−992.47021
TS_{22dc}	−205.389787	−205.31500	−205.30970	−205.34138	−319.59826	−205.37655	−205.30157	−205.29627	−205.32787	−300.40345

*E_{SCF}, U (thermal energy), H (thermal enthalpy), G (Gibbs free energy) (in au)

to form M_2; Path 5: M_2, by the cleavage of two weaker hydrogen bondings (1.856 Å and 2.147 Å), decomposes into M_{21} and M_{22} ; Path 6: M_{21}, by proton transfer of the G^+ cation, forms M_{21sp}; Path 7: M_{21sp}, by the destruction of intermolecular hydrogen bondings (1.680 Å and 2.107 Å), decomposes into M_{211} and M_{22}; Path 8: M_{22} executes bond breaking and rearrangement of C, N, and H atoms to obtain M_{22SP}; Path 9: M_{22SP} overcomes van der Waals forces (3.052 Å and 4.644 Å) to release an N_2 molecule, and forms M_{221}; Path 10: M_{211} cracks in three ways—first, by cracking one end of M_{211}, second, by cracking both ends of M_{211}, and finally, by cleaving the center of=N–N=—to obtain the same result of M_{211sp}, which is composed of two N_2 molecules and two HNC molecules with van der Waals forces and hydrogen bonding (3.855 Å, 2.170 Å) to form two straight lines, a $(N{\equiv}N\cdots HNC)_2$ molecule; Path 11: M_{211sp} overcomes van der Waals forces and hydrogen bonding (3.855 Å, 2.170 Å) to obtain two N_2 molecules and two linear HNC molecules; Path 12: HNC undergoes rearrangement to obtain HCN; Path 13: M_{221} (CH_3NH_2) undergoes dehydrogenation to obtain CH_2NH and H_2; Path 14: CH_2NH undergoes dehydrogenation to obtain HCN and H_2; Path 15: N_2 and H_2 react to form NH_3. Only five transition states were successfully calculated and were obtained in path 1, path 3, path 5, path 6, and path 8.

Decomposition pathways

The corresponding energies (ΔH and ΔG) in the 15 reaction paths are shown in Table 2. If the decomposition mechanism of GZT is suggested by reaction paths 1 to 11, then the net equation of the chemical reaction is expressed as Eq. (1):

$$M_0 \rightarrow 6N_2 + 2HNC + 2CH_3NH_2 \quad (1)$$

Table 4 Thermodynamic energy of transition state reaction

Reaction	Ea (kJ mol^{-1})	ΔH (kJ mol^{-1})	ΔG (kJ mol^{-1})
(1)$M_0 \rightarrow TS_{01} \rightarrow M_1\text{-}N_2$	[b]159.47	78.26	42.61
	[c]157.19	86.20	56.41
(3)$M_1 \rightarrow TS_{12dc} \rightarrow M_2\text{-}N_2$	184.78	102.28	66.62
	187.75	117.58	86.38
(5)$M_2 \rightarrow TS_{2dc} \rightarrow M_{21}+M_{22}$	40.01	31.70	10.46
	42.83	33.10	3.24
(6)$M_{21} \rightarrow TS_{21dc} \rightarrow M_{21sp}$	39.93	12.79	12.46
	37.78	11.99	10.82
(8)$M_{22} \rightarrow TS_{22dc} \rightarrow M_{22sp}$	25.25	22.08	59.02
	30.60	32.49	62.09

[b] B3LYP/6-31+G(2d,p) [c] B3LYP/6-31G(d,p) calculated method

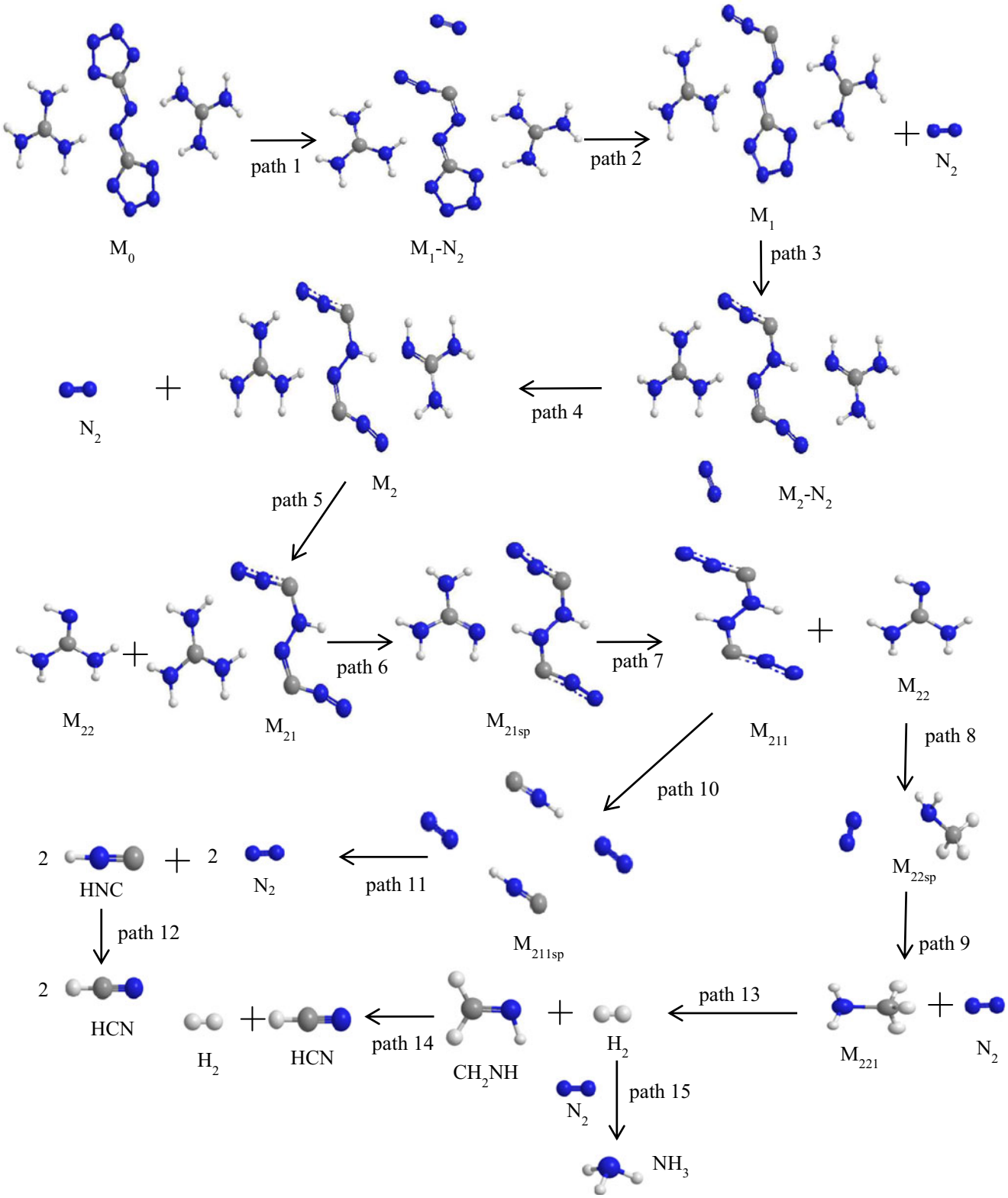

Fig. 5 Scheme of the decomposition reaction paths of GZT

The ΔH and ΔG values in Eq. (1) are −416.9, and −830.6 kJ mol^{-1}, respectively. The other four possible mechanisms are suggested by reaction paths 1 to 12, paths 1 to 13, paths 1 to 14, and paths 1 to 15, respectively. Their corresponding chemical

Table 5 Thermodynamic energy of decomposition net reactions of GZT

Reaction	Net reaction	B3LYP/6-311+G(d,p)			B3LYP/6-31+G(2d,p)			B3LYP/6-31G(d,p)		
		*ΔU (0K)	ΔH (298K)	ΔG (298K)	ΔU (0K)	ΔH (298K)	ΔG (298K)	ΔU (0K)	ΔH (298K)	ΔG (298K)
(1) path 1- 11	M_0=6 N_2+2 HNC+2 CH_3NH_2	−454.9	−416.9	−830.6	−361.6	−323.9	−738.6	−295	−257.2	−671.6
(2) path 1- 12	M_0=6 N_2+2 HCN+2 CH_3NH_2	−560.9	−525.1	−935.6	−467.9	−431.8	−844.1	−419.4	−383.3	−795.3
(3) path 1- 13	M_0=6 N_2+2 HCN+2 CH_2NH+2 H_2	−364.9	−314.5	−794.6	−266.3	−202.5	−683.8	−221.6	−170.7	−652.7
(4) path 1- 14	M_0=6 N_2+4 HCN+4 H2	−272.6	−206.8	−749.2	−168.3	−87.4	−634.9	−132.4	−66.1	−610.5
(5) path 1- 15	M_0=5 N_2+4 HCN+H_2+2 NH_3	−358.6	−307.5	−796.5	−263.7	−212.1	−703.2	−192.9	−141.3	−632.2

*ΔU (thermal energy), ΔH (thermal enthalpy), ΔG (Gibbs free energy) (in kJ mol^{-1})

equations are expressed as Eqs. (2), (3), (4) and (5):

$$M_0 \rightarrow 6N_2 + 2HCN + 2CH_3NH_2 \quad (2)$$

$$M_0 \rightarrow 6N_2 + 2HCN + 2H_2 + 2CH_2NH \quad (3)$$

$$M_0 \rightarrow 6N_2 + 4HCN + 4H_2 \quad (4)$$

$$M_0 \rightarrow 5N_2 + 4HCN + H_2 + 2NH_3 \quad (5)$$

The ΔH and ΔG values for the above possible decomposition reactions are shown in Table 5. Table 5 reveals that ΔH and ΔG of all five possible decomposition reactions [Eqs. (1), (2), (3), (4) and (5)] are negative. These results indicate that N_2, HNC, CH_3NH_2, HCN, H_2, CH_2NH, and NH_3 can be produced by spontaneous exothermic reaction (1)-(5). The order of the negative values of ΔH and ΔG in these five exothermic reactions is reaction (2)>reaction (1)>reaction (3)>reaction (5)>reaction (4); hence, reaction (2) is much more favored than the other four possible decomposition reactions. Table 2 shows that CH_3NH_2 and CH_2NH undergo dehydrogenation requiring large amounts of energy of 329.7 kJ mol^{-1} and 107.4 kJ mol^{-1}, respectively, in path 13 and path 14. This caused the ΔH values to decrease for reactions (3)–(4) in Table 5. Some of the N_2 and H_2 molecules formed in the decomposition process react to produce NH_3 molecules in the explosive (i.e., high-temperature, high-pressure) environment. In this study, five possible decomposition reactions were found to occur, and final products such as N_2, HCN, and NH_3 molecules were obtained; these final product results are consistent with those of experiments examining the decomposition reactions of GZT (also named GAT, or GAZ) [20, 21, 23, 24]. In order to prove the reliability of the above-mentioned results, the observed data were selected from one of the standard infrared spectra textbook [36] as shown in Table 6 for theoretical comparison. Table 6 reveals that theoretically-calculated chemical vibrational frequencies such as C≡N stretching (2106 cm^{-1}) and C–H stretching (3315 cm^{-1}) of HCN, and N–H asymmetric stretching (3445 cm^{-1}) and N–H symmetric stretching (3350 cm^{-1}) of NH_3, agree with the standard infrared spectra textbook [36]; the error in the bond vibrational frequencies is only 0.09%–0.9% and 0.20%–2.5% for HCN and NH_3 molecules, respectively. The IR spectra of NH_3 and HCN are shown in Fig. 6.

Table 6 The IR spectra data of HCN and NH_3 molecules

Vibration type	HCN			NH_3			
	#ν_{obs} (cm^{-1})	*νcal (cm^{-1})	Error(%)	Vibration type	ν_{obs} (cm^{-1})	νcal (cm^{-1})	Error(%)
C-H out of planer bending	712	719	0.9%	N-H out of planer bending	968	993	2.5%
C-H in planer bending	1412	-	-	N-H in planer bending	1627	1604	1.4%
C≡N streching	2089	2106	0.8%	N-H symmetric streching	3337	3350	0.2%
C-H streching	3312	3315	0.09%	N-H asymmetric streching	3414	3445	0.9%

obs. extract from ref [36];. *ν_{cal} (cm^{-1}) B3LYP/6-311+G(d,p) calculated results scaled by 0.96 at B3LYP ref [45]

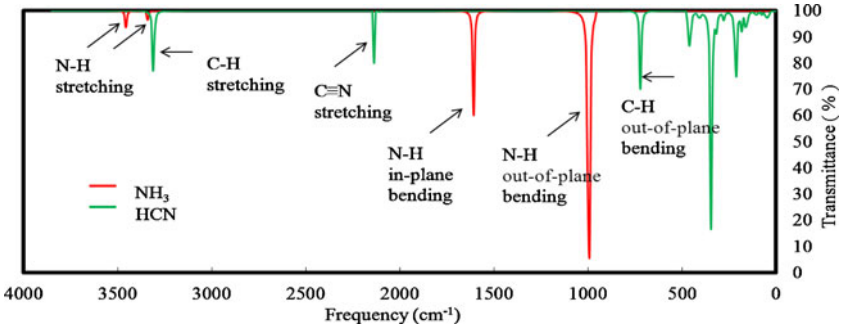

Fig. 6 IR spectra of HCN and NH_3 of the final decomposition products of GZT; B3LYP/6-311+G (d,p) calculated results

Thermodynamic property analysis

From the point of view of thermodynamics, ΔH and ΔG are very important quantities of chemical reactions for highly energetic materials. It is especially difficult to obtain experimental thermal chemical data of each elementary reaction of the decomposition mechanism for the highly energetic molecule GZT. For this reason, theoretical prediction of ΔH and ΔG is very important. Thermodynamic data obtained from theoretical calculations using the density functional theory B3LYP with three basis set methods at 0 and 298 K are listed in Tables 2 and 4. Table 2 reveals that six reactions are endothermic and nonspontaneous, which are reaction paths 1, 3, 6, 7, 13, 14. Nine reactions are spontaneous, because ΔG is less than zero, which are reaction paths 2, 4, 5, 8, 9, 10, 11, 12, 15. Paths 2, 4, 5, 11 are endothermic reactions but reaction paths 8, 9, 10, 12, 15 are exothermic. There are many differences in the theoretical calculations among the three basis set methods. From Table 2, it is interesting to observe that the largest amounts of energy were released spontaneously in reaction path 10, and the ΔH and ΔG values are −598.3 kJ mol^{-1} and −656.4 kJ mol^{-1} with B3LYP/6-311+G(d,p), respectively, which are higher than those with B3LYP/6-31+G(2d,p) and B3LYP/6-31G(d,p). This information indicated that GZT can release large amounts of energy, the main contribution being from the disintegration of the 5, 5'-azotetrazolate anion (ZT^{2-}) skeleton (ΔH=−598.3 kJ mol^{-1}), and it also explains the reason for which many 5,5'-azotetrazolate salts are highly energetic compounds [37–44]. The activation energies of the five transition states and the thermodynamic energies (ΔH, ΔG) for each reaction path are listed in Table 4. The data in Table 4 indicate that the activation energy of the first ring opening in reaction path 1 was 159.5 kJ mol^{-1}. An even higher activation energy was required for the second ring opening decomposition, the energy required being 184.8 kJ mol^{-1}. These results also reveal that the molecular-type cracking patterns decomposition mechanism of GZT proposed herein is a plausible decomposition path, the activation energies required being lower than those of the ion-type decomposition mechanism [27]. It is very difficult to determine the quantity distribution among the five possible net decomposition reactions of GZT. Therefore, we chose the largest negative value of ΔH of Eq. (2), which compares with the result obtained in the experiment. In Table 5, the largest negative value of ΔH for the chemical reaction shown in Eq. (2) is −525.1 kJ mol^{-1} (−441.87 kJ/kg), which closely approaches the value of molar enthalpy (−426.1 kJ/kg) for the GZT detonation experiment conducted by Hammel et al. [20]. From the qualitative or quantitative point of view, these simulation calculations are important and suggest that the GZT decomposition mechanism is a feasible and spontaneous exothermic reaction.

Conclusions

In this study, three basis set methods of the Gaussian 03 package were used to successfully complete a prediction of the possible reaction path and calculation of the thermodynamic properties of GZT decomposition. Four important conclusions were obtained:

(1) The optimized geometric structures of the intermediates, transition states, and final products obtained in this theoretical simulation are available, so that detailed elementary reactions that cannot be observed in the real experiments can be explored.
(2) It was confirmed that GZT can release large amounts of energy, with the disintegration of the 5,5'-azotetrazolate anion (ZT^{2-}) skeleton being the main contributor.
(3) Thermodynamic properties from calculations using the B3LYP/6-311+G(d,p) method closely approach the experimental values of the thermal decomposition of GZT.
(4) The final products are N_2, HCN, and NH_3, and their IR spectra obtained from the simulation calculations are consistent with experimental measurements.

By research to construct the complete decomposition path of GZT, by exploration of simulation studies, and by comparison with experiments, a precise method was developed to predict the decomposition reaction mechanisms of GZT derivatives such as AGZT, DAGZT, and TAGZT.

Acknowledgments The authors would like to thank the National Center for High-Performance Computing for performing the calculations.

References

1. Bucerius KM (1993) Stable nitrogen-rich composition: U.S. Pat. 5,198,046
2. Thiele J (1892) Ueber nitro-und amidoguanidin. Justus Liebigs Ann Chem 270:1–63
3. Hiskey MA, Goldman N, Stine JR (1998) High-nitrogen energetic materials derived from azotetrazolate. J Energ Mater 16:119–127
4. Hammerl A, Holl G, Kaiser M, Klapötke TM et al (2001) Methylated Ammonium and Hydrazinium Salts of 5,5'-azotetrazolate. Z Naturforsch 56:847–856
5. Yang SQ, Yue ST (2003) Progress in high-nitrogen energetic materials derived from tetrazine and tetrazole. Chin J Energ Mater 11:231–235
6. Yang SQ, Xu SL, Lei YP (2006) Development of nitrogen heterocyclic energetic compounds. Chin J Energ Mater 14:475–484
7. Bucerius KM, Eisenreich N, Schmid H, Engel W (1997) Gas generating mixture containing copper diammine dinitrate. U.S. Pat. 5,663,524
8. Schmid H, Eisenreich N (2000) Investigation of a two-stage airbag module with azide-free gas generators. Propellants Explos Pyrotech 25:230–235
9. Khandhadia PS, Burns SP (2001) Thermally stable nonazide automotive airbag propellants. US 6:306,232
10. Walsh CM, Knott CD, Leveritt CS (2006) Reduced erosion additive for a propelling charge. US 6:984,275
11. Hudson MK, Wright AM, Luchini C, Wynne PC et al (2004) Guanidinium Azo-Tetrazolate (GAT) as a High Performance Hybrid Rocket Fuel Additive. J Pyrotech 19:37–42
12. Damse RS, Siker AK (2009) Suitability of nitrogen rich compounds for gun propellant formulations. J Hazard Mater 166:967–971
13. Peng YL, Wong CW (1999) Preparation guanidinium 5,5'-azotetrazolate. U.S. Pat. 5,877,300
14. Hammerl A, Holl G, Klapötke TM, Mayer P et al (2002) Salts of 5,5'-azotetrazolate. Eur J Inorg Chem 4:834–845
15. Bucerius KM (1992) Guanidinium-5,5'-azo-tetrazolate - is stable nitrogen-rich cpd. yielding non-harmful gases upon decomposition. Ger. Pat. DE4,034,645
16. Bucerius KM, Wasmann FW, Menke K (1991) Pyrotechnical compositions for the generation of environmentally safe, nontoxic gases. Ger. Pat. DE4,108,225
17. Xu SL, Yang SQ (2006) Synthesis and properties of high-nitrogen energetic compounds based on azotetrazolate nonmetallic salts. Chin J Energ Mater 14:377–340
18. Xu SL, Yang SQ, Yue ST (2005) Synthesis and characterization of high-nitrogen energetic compounds derived from azotetrazolate. Chin J Explos Propell 28:52–55
19. Wang HS, Du ZM (2005) Progress in synthesis and properties of nitrogen-rich compounds. Chin J Energ Mater 13:196–199
20. Hammerl A, Hiskey MA, Holl G, Klapötke TM (2005) Azidoforma-midinium and guanidinium 5,5'-Azotetrazolate Salts. Chem Mater 17:3784–3793
21. Sivabalan R, Talawar MB, Senthilkumar N, Kavitha B et al (2004) Studies on azotetrazolate based high nitrogen content high energy materials potential additives for rocket propellants. J Them Anal Calorim 78:781–792
22. Damse RS, Naik NH, Ghosh M, Venugopalan S (2007) Structure-decomposition mechanism relationship for the energetic nitrogen rich compounds. 38th International Annual Conference of ICT 79-1-79-12
23. Tappan BC, Ali AN, Son SF, Brill TB (2006) Decomposition and Ignition of the High-Nitrogen Compound Triaminoguanidinium Azotetrazolate (TAGzT). Propell Explos Pyrot 31:163–168
24. Damse RS, Naik NH, Ghosh M, Sikder AK (2009) Thermoanalytical Screening of Nitrogen-Rich Compounds for Ballistic Requirements of Gun Propellant. J Propul Power 25:249–256
25. Miyata Y, Hasue K (2013) Thermal decomposition of aminoguanidinium 5,5'-azobis-1H-tetrazolate. Thermochim Acta 553:68–77
26. Alavi S, Reilly LM, Thompson DL (2003) Theoretical predictions of the decomposition mechanism of 1, 3, 3-trinitroazetidine (TNAZ). J Chem Phys 119:8297–8304
27. Liu MH, Cheng SR, Cheng KF, Chen C (2008) Kinetics of decomposition pathways of an energetic GZT molecule. Int J Quant Chem 108:482–486
28. Chen C, Liu MH, Cheng SR, Wu LS (2003) Theoretical study of the inter-ionic hydrogen bonding in the GZT molecular system. J Chin Chem Soc 50:765–775
29. Cheng C, Liu MH, Liu CW (2004) Theoretical study of the inter-ionic and inter-molecular hydrogen bonds constructed by GZT, ZT^{2-} ions and their relative derivatives. J Mol Struct (THEOCHEM) 685:163–174
30. Storm CB, Ryan RR, Ritchie JP, Hall JH et al (1989) Structural Basis of the Impact Sensitivities of I-Picryl-I,2,3-triazole, 2-Picryl-I,2,3-triazole, 4-Nitro-I-picryl-I,2,3-triazole, and 4-Nitro-2-picryl-I,2,3-triazole. J Phys Chem 93:1000–1007
31. Politzer P, Grice ME, Seminario JM (1997) Density Functional Analysis of a Decomposition of 4-Nitro-1, 2, 3- Triazole Through the Evolution of N_2. Int J Quant Chem 61:389–392
32. Frisch MJ, Trucks GW, Schlegel HB, Scuseria GE (2003) Gaussian 03, Revision B.03. Gaussian, Inc, Pittsburgh
33. Lee C, Yang W, Parr RG (1988) Development of the Colle-Salvetti Correlation-energy Formula into a Functional of the Electron Density. Phys Rev B37:785–789
34. Peng C, Schlegel HB (1993) Combining Synchronous Transit and Quasi-Newton Methods to Find Transition States. Israel J Chem 33:449–454
35. Peng C, Ayala PY, Schlegel HB, Frisch MJ (1998) Using Redundant Internal Coordinates to Optimize Equilibrium Geometries and Transition States. J Comput Chem 17:49–56
36. Herzberg G (1966) Infrared and Raman Spectra of Polyatomic Molecules. Florida, USA 279–295
37. Hammerl A, Klapötke TM, Nöth H, Warchhold M (2001) $[N2H5]^{+2}[N4C-N=N-CN4]^{2-}$: A New High-Nitrogen High-Energetic Material. Inorg Chem 40:3570–3575
38. Klapötke TM, Sabaté CM (2008) Bistetrazoles: Nitrogen-Rich, High-Performing, Insensitive Energetic Compounds. J Chem Mater 20:3629–3637
39. Klapötke TM, Sabaté CM (2008) Nitrogen-Rich Tetrazolium Azotetrazolate Salts: A New Family of Insensitive Energetic Materials. J Chem Mater 20:1750–1763
40. Sivabalan R, Anniyappan M, Pawar SJ, Talawar MB et al (2006) Synthesis, characterization and thermolysis studies on triazole and tetrazole based high nitrogen content high energy materials. J Hazard Mater A137:672–680
41. Fischer N, Klapötke TM, Scheutzow S, Stierstorfer J (2008) Hydrazinium 5-Aminotetrazolate: an Insensitive Energetic Material Containing 83.72% Nitrogen. Cent Eur J Energ Mater 5:3–18
42. Warner KF, Granholm HG (2011) Synthesis of Insensitive 5,5'-Azotetrazolate Salts. J Energ Mater 29:1–6
43. Klapötke TM, Miró Sabaté C (2009) New energetic compounds based on the nitrogen-rich 5,5′-azotetrazolate anion ($[C_2N_{10}]^{2-}$). New J Chem 33:1605–1617
44. Laus G, Kahlenberg V, Wurst K, Schottenberger H et al (2012) Synthesis and Crystal Structures of New 5,5'-Azotetrazolates Crystals 2:127–136
45. Lin TP, Chen C (2000) Vibrational Study of Pyrazole Molecule. J Chin Chem Society 58:591–596